Defense Technical Information Center
Compilation Part Notice

ADP014103

TITLE: Prediction the Jet Near-Field Noise of Combat Aircraft

DISTRIBUTION: Approved for public release, distribution unlimited
Availability: Hard copy only.

This paper is part of the following report:

TITLE: Aging Mechanisms and Control. Symposium Part A -
Developments in Computational Aero- and Hydro-Acoustics. Symposium
Part B - Monitoring and Management of Gas Turbine Fleets for Extended
Life and Reduced Costs [Les mecanismes vieillissants et le controle]
[Symposium Partie A - Developpements dans le domaine de
l'aeroacoustique et l'hydroacoustique numeriques] [Symposium Partie B ...

To order the complete compilation report, use: ADA415749

The component part is provided here to allow users access to individually authored sections
of proceedings, annals, symposia, etc. However, the component should be considered within
the context of the overall compilation report and not as a stand-alone technical report.

The following component part numbers comprise the compilation report:
ADP014092 thru ADP014141

Predicting the Jet Near-Field Noise of Combat Aircraft

M. Harper-Bourne
QinetiQ, Farnborough, Hampshire
GU14 0LX, UK

Abstract

QinetiQ (previously DERA) is currently undertaking on behalf of the UK MOD an integrated programme of applied research to develop improved prediction methods for acoustic fatigue assessment on next generation combat aircraft. This paper describes ongoing work to develop practical methods of predicting the near-field noise of the high-speed exhausts of military jet engines, for use at an engineeering level. The study encompasses both jet mixing noise and broadband shock noise for single and twin jets and is focussed on predicting the intensity, spectra and spatial coherence of jet noise at the airframe, using a semi-empirical basis that marries aeroacoustic theory with source location data. The background to the development of the method through small scale heated model noise tests in the QinetiQ Noise Test Facility is described, followed by validation through near-field noise tests conducted in the QinetiQ GLEN sea-level engine test facility on a Rolls-Royce Spey turbojet engine.

1. Introduction

Advances in the propulsion and airframe technology of combat aircraft have highlighted deficiencies in current knowledge of acoustic fatigue prediction (Ref. 1). These prevail in three areas. Firstly, in the pursuit of increased combat efficiency higher specific thrust engines are being developed producing higher levels of jet noise, further reducing the fatigue life of airframe and systems. Secondly, novel airframe and propulsion configurations are being adopted (e.g. JSF) that demand more advanced tools for the prediction of acoustic loading. Finally, new strategic requirements such as stealth, ASTOVL, supermanouverability and supercruise are resulting in the adoption of novel materials and lighter constructional techniques that must withstand the escalating jet noise environment. In combat, relatively small cracks in an aircraft's RAM could make it and its aircrew fatally vulnerable to attack by BVR missiles, for example.

The present paper reports ongoing research, being undertaken by QinetiQ for the UK MOD, to model the forcing functions of jet exhaust near-field noise (Fig. 1) essential to structural assessment, inparticular prediction of the exposure to the jet noise field in terms of overall level, spectral content and spatial coherence. The research is encompassing the primary noise sources of military turbojet exhausts, namely, jet mixing noise, Mach wave radiation and shock noise. A semi-empirical approach to modelling the noise sources has been adopted in order to provide practical engineering design aid tools within realistic time scales. The methodology combines classical aeroacoustic theory with measured source location data, enabling the noise field close to the jet to be defined spatially. The underlying source data is measured on (typically) 1/12th scale heated air jets (single and twin). The developed methods are being validated against full scale engine near-field noise measurements, an example of which is presented.

2. Near-field Research Programme

In general, use of sub-scale test data in aeroacoustics is well proven and has obvious cost benefits over full-scale engine tests, which can be reserved for model validation. For this work, the QinetiQ Noise Test Facility (NTF) at Pyestock, which is a unique world class noise measurement facility specifically designed for jet exhaust noise research, is being used. The facility permits the anechoic testing at model scale hot, high velocity, conditions representative of combat aircraft, with forward flight simulation if required. The need for a hot testing capability in jet noise research cannot be overemphasised as temperature determines the relative balance of the different noise sources present in the exhaust of a turbojet engine. In addition, model scale anechoic testing permits the individual components of jet noise to be studied, which would be impractical in engine tests. This flexibility provides scope for a more fundamental understanding of the noise mechanisms and the possibility of developing methods for the amelioration of jet noise.

The fundamental mechanisms of military jet engine noise, if not fully understood are at least well known (Ref. 2). In addition to the primary jet noise sources of Fig 1, it is intended that the jet noise modelling should address all of the features listed on Fig. 2, which includes relevant configuration and operational aspects. Of the noise sources, shock screech, which is a common feature at model scale, is rarely observed at full scale but may be relevant to the modelling of missile exhausts.

Generated within the engine, core noise needs to be identified and quantified directly from engine exhaust measurements. In the near-field it is also necessary to consider the hydrodynamic perturbations of the turbulent eddies in the exhaust (Fig. 3),which can be done at model scale. The hydrodynamic field does not propagate as sound but needs to be considered, along with the acoustic elements, when considering the nozzle structure, or when the exhaust is close to, or scrubbing, the airframe such as with buried 'stealthy' type propulsion nozzle systems. For the interaction of noise with the airframe, a proprietary boundary element method (Ref. 3) is proposed for use with the free field models of the current work.
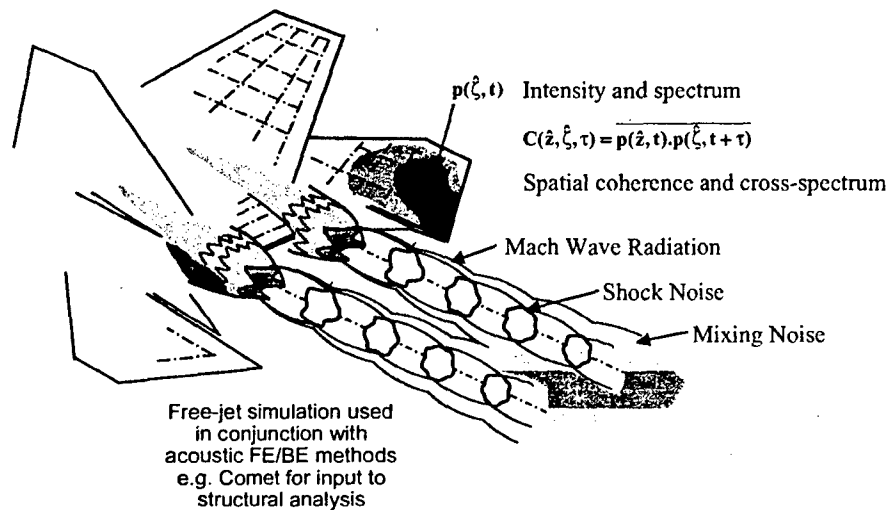

$p(\zeta,t)$ Intensity and spectrum

$$C(\hat{z},\zeta,\tau) = \overline{p(\hat{z},t).p(\zeta,t+\tau)}$$

Spatial coherence and cross-spectrum

Mach Wave Radiation

Shock Noise

Mixing Noise

Free-jet simulation used in conjunction with acoustic FE/BE methods e.g. Comet for input to structural analysis

Fig.1 Combat Aircraft Jet Noise Sources

The fact that a jet flow is a spatially distributed noise source has significant implications when predicting jet near-field noise. The spatial extent of the sources along the jet and their frequency dependence can be determined using an acoustic imaging technique such as Polar Correlation (Refs. 4 and 5) illustrated in Fig. 4. This sound field analysis technique was developed originally to provide a source location capability for use on full scale engines for Rolls-Royce.

Mixing Noise
Eddy Mach Wave
Shock Noise
Screech
Hydrodynamic
Core Noise

Single Jet
Twin Jet
Thrust Vectoring
LO / Stealth
ASTOVL

Reheat
Altitude / Mach No.
Forming Effect

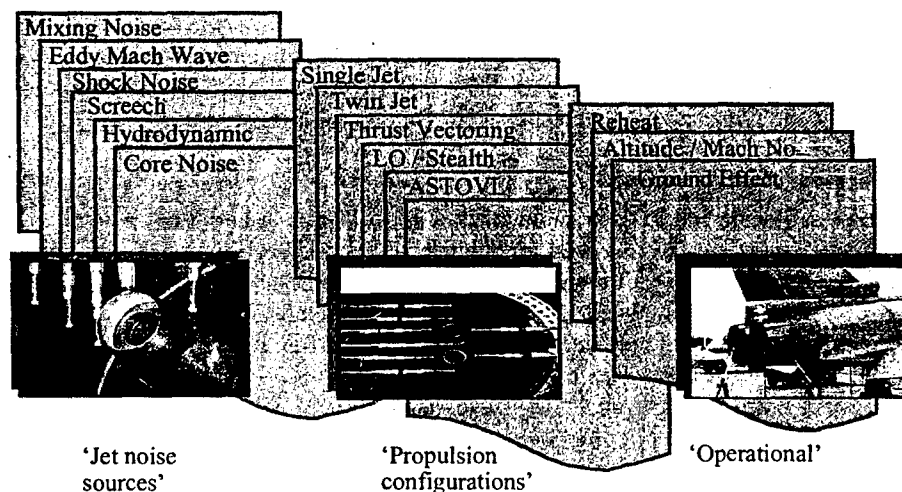'Jet noise sources'   'Propulsion configurations'   'Operational'

Fig.2 Near-Field Noise Research Programme

However, Polar Correlation is relatively expensive and time consuming and in order to provide a simple low cost source location capability for basic research at model scale, a wide angle (1.3m diameter) elliptic

mirror has been developed (Fig. 5a). Sound at the outer focal point is collected by the mirror and focussed onto a microphone (Fig. 5b) at the inner focal point. A motorised three-axis traverse allows the source distributions within a jet to be readily surveyed and sources separated by as little as one wavelength can be resolved.

Conical Nozzle

X =6.4D, Y = 4.2D, K=27dB, Nozzle Diameter = 36 mm

U_j/a_0	OASPL
1.228,	145.7 dB
1.134,	142.3 dB
1.057,	138.3 dB
0.996,	132.5 dB
0.825,	124.3 dB
0.575,	112 dB
0.407,	103.6 dB
0.28,	93 dB
0.15,	85 dB

Shock noise

Mixing noise

Hydrodynamic
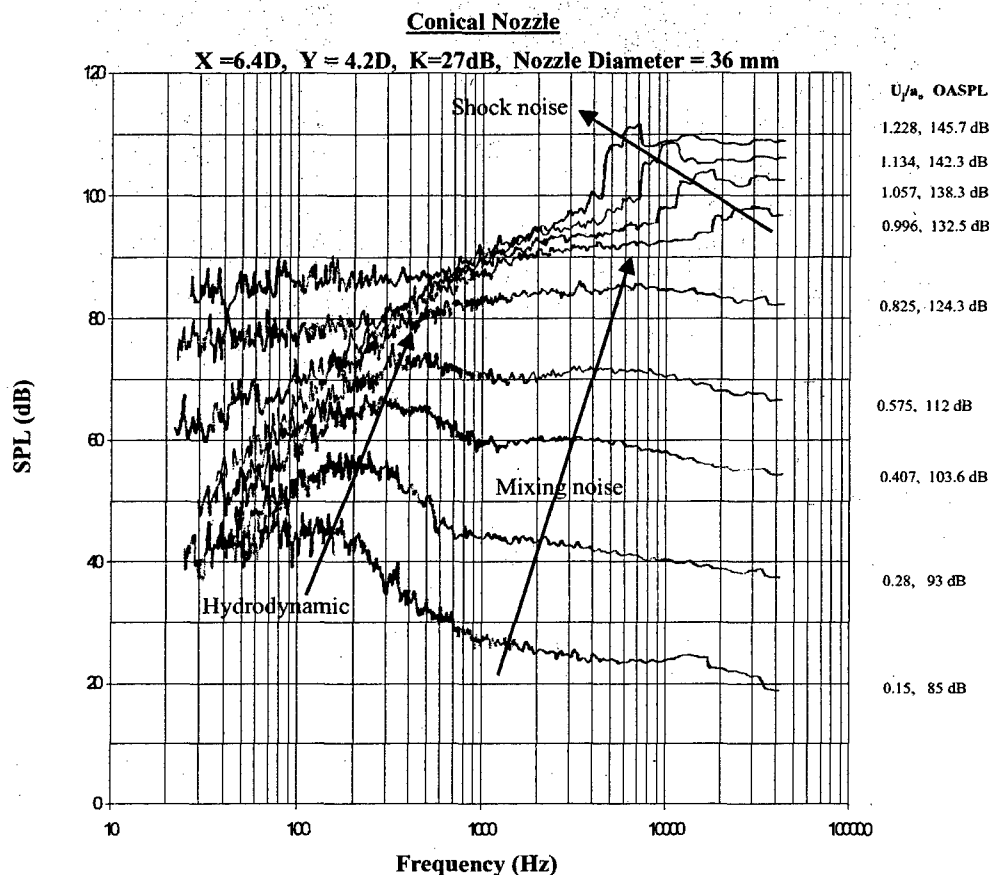
Fig.3 Near-Field 1/3rd Oct. Spectra for 36mm Model Jet

AXIAL SOURCE DISTRIBUTION

NEAR-FIELD

FOURIER TRANSFORM

COHERENCE AND PHASE

FAR-FIELD

Nozzle
Y_1 - Jet Axis
Jet flow
α
Y_2
r_2
r_0
r_1
r_θ
M_2
Traversable microphone
M_1
G(τ)
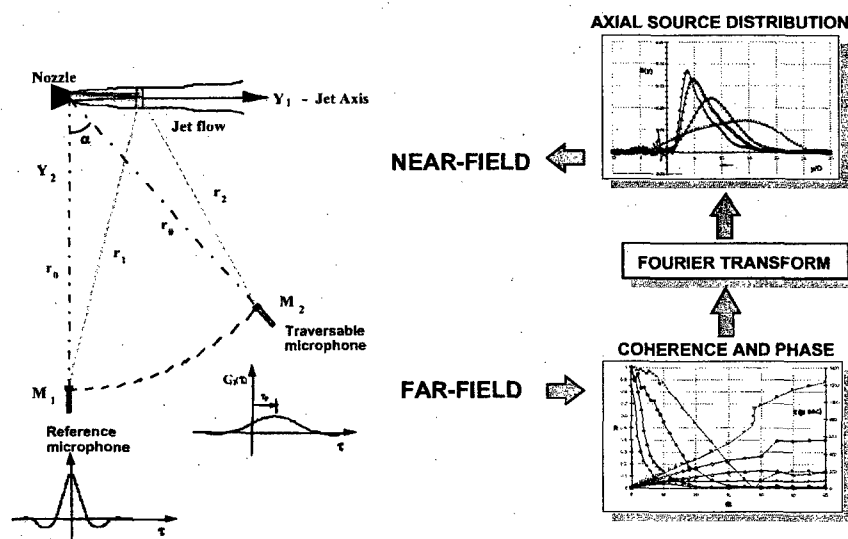Reference microphone

Fig.4 Polar Correlation

Typical results for an underexpanded convergent nozzle are presented in Fig. 6, which clearly shows the peaks indicating the presence of the shock cells. These measurements have also helped confirm fundamental aspects of the shock noise model such as the discrete or concentrated form of the individual shock noise sources
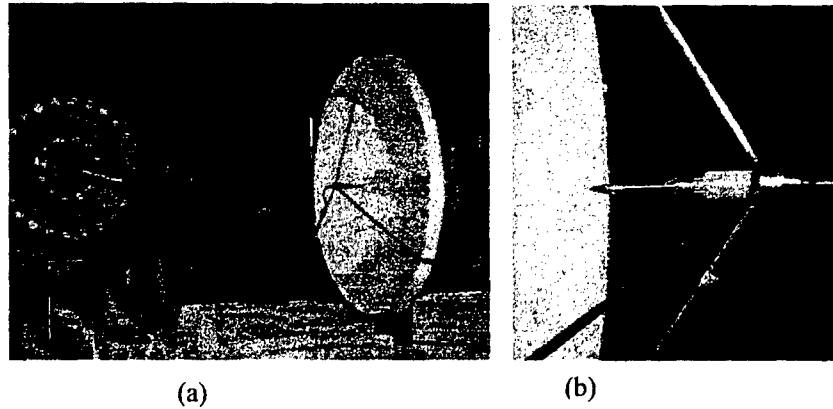

(a)   (b)

Fig.5 NTF Acoustic Mirror

3.   Near-Field Modelling

3.1 Jet Mixing Noise

Lighthill's quadrupole theory of jet mixing noise (Ref. 6), yields for the far-field acoustic pressure

$$p(\hat{x}, t) = \frac{1}{4\pi a_0^2} \int_{\hat{y}} \ddot{T}_{rr}(\hat{y}, t - r/a_0)\frac{dV}{r} \tag{1}$$

where $T_{rr} = \rho U_r^2 + \{p - a_0\rho\}$ is the Proudman form of the Lighthill quadrupole stress, i.e resolved in the direction of the observer (Fig. 7). In Ref. 7 it is shown that the near-field of a quadrupole element has the general form:

$$p \propto \frac{[\ddot{T}]}{a_0^2 r} + \frac{3[\dot{T}]}{a_0 r^2} + \frac{3[T]}{r^3} \tag{2}$$

The second and third terms in eqn. 2 are non-conservative and relate to the hydrodynamic component identified in Fig 3, while the first term is responsible for the near-field acoustic component. It therefore follows that eqn. 1 is also valid for the near-field acoustic pressure of a jet flow, as well as the far-field. For the high speed jet flows considered in the present work the term $\{p - a_0\rho\}$, responsible for entropy noise (Ref. 8), is assumed negligible and ignored here.

Starting with the power spectral density of the acoustic near-field, in Ref. 9 a generic form is derived for the self noise of a jet using two-point space-time turbulence correlation measurements in eqn. 1. This exercise, undertaken in a fixed frame of reference, yields the following for the power spectral density (psd) of the mixing noise at point $\hat{z}$ (microphone M1) in Fig. 7:

$$G_1(\omega) = \frac{1}{\left(4\pi a_0^2\right)^2} \int_{y_1} S_r(y_1, \theta, \omega)\frac{dy_1}{r_1^2} \tag{3}$$

S_r is the source strength per unit slice of jet at the axial station y_1 for the radian frequency $\omega(=2\pi f)$ in the direction of field point $\hat{z}$ and is given by

$$S_r(y_1, \omega, \theta) = G_{90}(\omega).D_p(y_1, \theta, \omega).C_A(y_1, s_d).S(y_1, \omega).D^2 \tag{4}$$

where: $G_{90}(\omega)$ is the far-field psd perpendicular to the jet axis, normalized to a radius of one nozzle diameter. $D_p(y_1, \theta, \omega)$ is the inherent directivity of the quadrupoles constituting the jet mixing noise sources, θ being the local angle to the jet axis of observation point $\hat{z}$ relative to the jet slice. $C_A(y_1, s_d)$ defines convective amplification (determined in a fixed frame of reference) resulting from the axial convection of the turbulent eddies within the jet shear layer and s_d is the Doppler shifted axial decay Strouhal number of the turbulence.

$S(y_1,\omega)$ is the normalized source strength density 90^0 to the jet axis, derived from source location measurements such as Polar Correlation or the acoustic mirror and is defined:

$$\int_0^\infty S(y_1,\omega)dy_1 = 1 \tag{5}$$

In Ref. 9, the lateral decay scales associated with self noise are shown to be acoustically compact and this permits the three dimensional form of eqn. 1 to be reduced to the axial line integral of eqn. 2. In Ref. 10, the one-dimensional form of eqn. 3 is shown to be acceptable providing $r_1 \geq D$ (stations closer than 1D are likely to incur errors exceeding 1dB).

For convective amplification, the fixed frame analysis of measured filtered turbulence space-time-correlations of Ref. 9 yields: $C_A(y_1,s_d) = \dfrac{1}{[1+s_d^2]^m}$ where $s_d = \dfrac{\omega L_1}{U_c}[1 - M_c \cos\theta]$ and typically m=1.5

The quantity $\omega L_1 / U_c$ is the local longitudinal turbulence decay Strouhal number (L_1 being the axial separation at which $R(\eta_1,\omega) = 1/e$). Each spatial source distribution has a dominant characteristic value determined by the jet Strouhal number $\omega D/U_j$. Note for s_d large, the convective amplification tends to three powers of the Doppler factor. Also, at the Mach angle $s_d = 0$, and the convective amplification factor is equal to unity (rather than the infinity of Lighthill's original analysis).
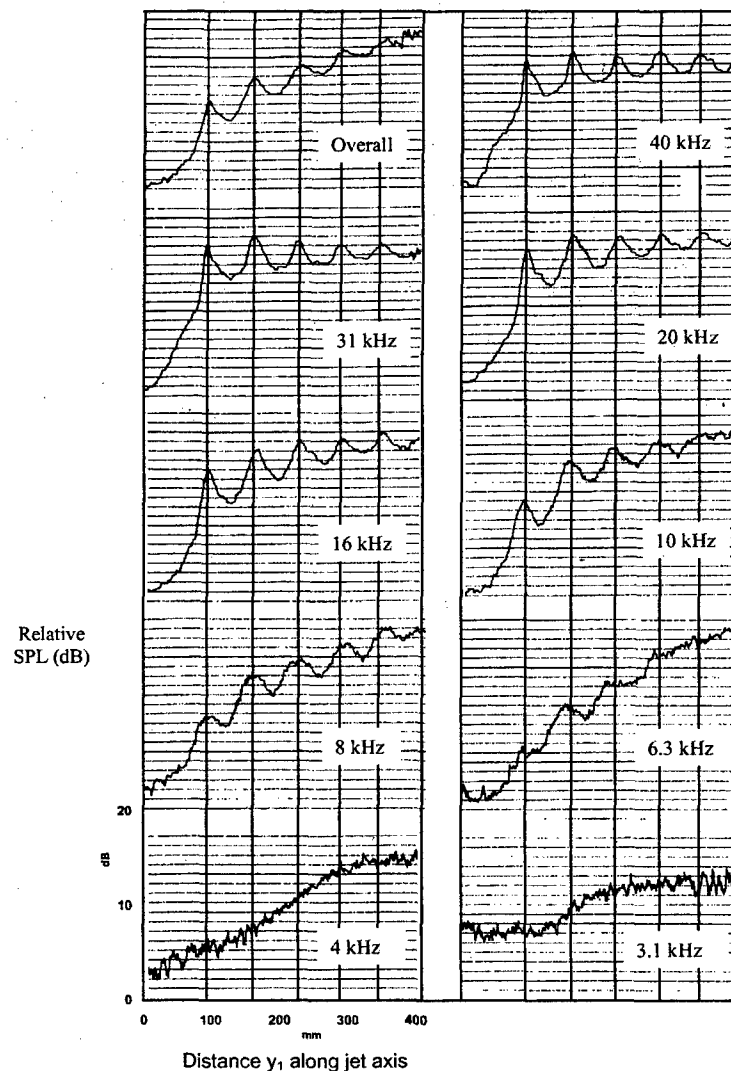

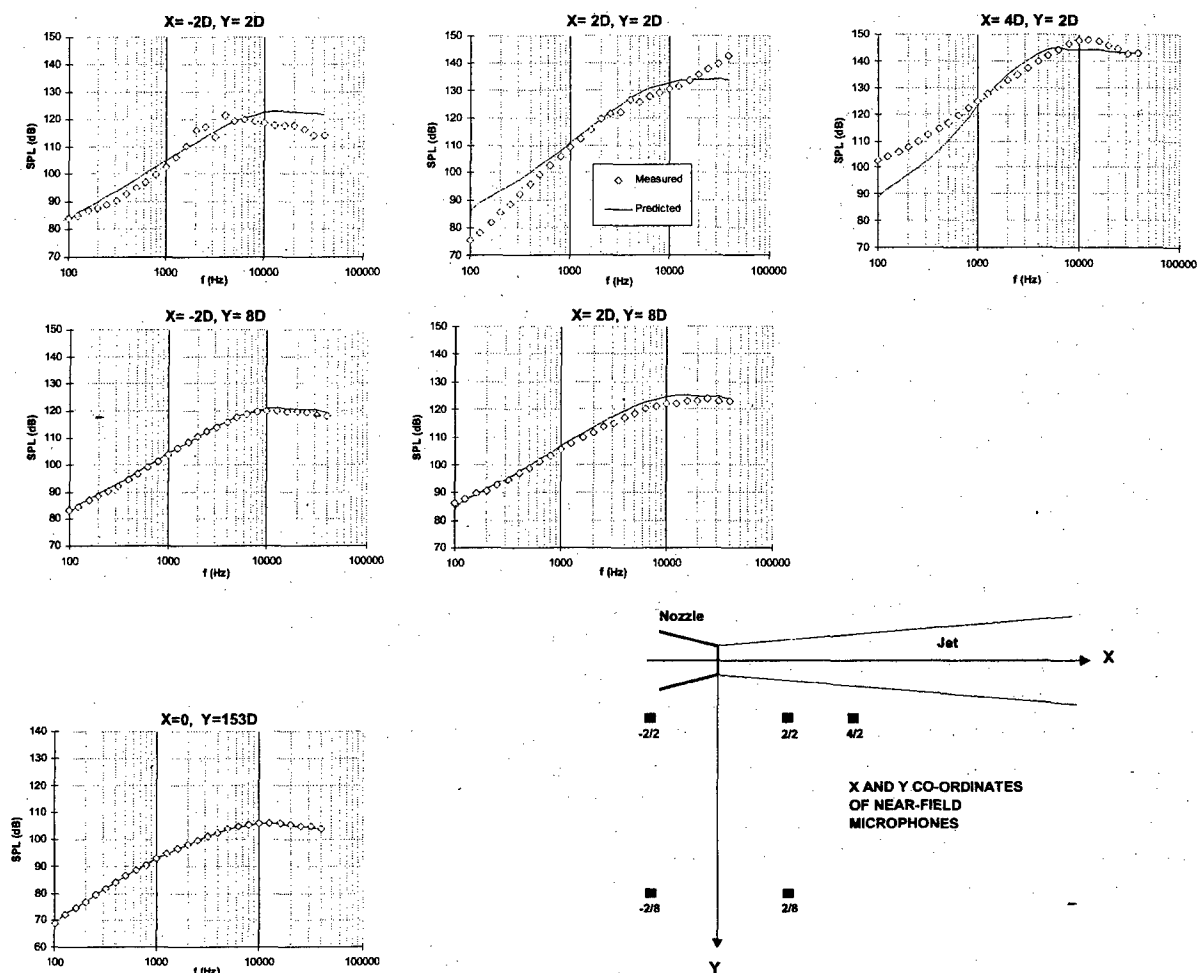*Fig.6 Mirror Axial Traverse, Underexpanded Jet, PR=3.7, 46 mm Conical Nozzle*

Fig.7 Co-ordinate System for Near-Field Analysis of Jet Mixing Noise

Typical source distributions for a range of jet Strouhal number are shown in Fig. 8 for a round convergent jet of velocity ratio $U_j/a_0 = 0.8$. These are shown as comprising two components educed from Polar Correlation measurements, one for the mixing region of the jet (red curve) and one for the fully developed downstream region (blue curve). The component curves take the form:

$$S_m(y_1,\omega) = W_m /[6Y_m].[y_1/Y_m]^3.e^{-y_1/Y_m} \text{ and } S_{fd}(y_1,\omega) = 2.W_{fd}/Y_{fd}.[y_1/Y_{fd}]^3.e^{-[y_1/Y_{fd}]^2}$$

where $Y_m = Y_{pm}/3.D$, $Y_{fd} = Y_{pfd}.D.[2/3]^{0.5}$ and $S(y_1,\omega) = S_m(y_1,\omega) + S_{fd}(y_1\omega)$. The quantities W and Y_p define the peak of each distribution and are functions of the jet Strouhal number $St = fD/U_i$

The effect of increasing Mach number M_j is to produce some stretching of the distributions. Where nozzle geometry, or some form of flow excitation, generates enhanced mixing, the distributions are likely to be shortened. Such an effect is described in Ref 10 for twin jets where a strong 'organ pipe' tone existed within the jet pipe at the Mach number under test. The result was increased broadband mixing noise whilst apparently shortening the source distributions by 50%.

Fig.8 Generic Axial Distributions of Jet Mixing Noise

Fig.9 Mixing Noise Predictions (M_j=1.5, T=885K, D=39mm Con-di Nozzle)

Using the generic maths model of eqns. 3 and 4, the near-field noise for any given jet size, combination of jets, jet velocity etc. can be predicted. In the case of multiple jets, Ref. 10 has revealed the need to incorporate the effects of jet shielding caused by refraction effects. However, this generally affects downstream stations away from the airframe.

Typical predictions using the model are compared with $1/3^{rd}$ octave noise spectral measurements in Fig. 9 for a heated fully expanded M1.5 jet, for three inner near-field stations (Y=2D), two outer near-field stations (Y=8D) and a farfield station (Y=150D, $\theta = 90^0$). Since the method uses the far-field 90^0 noise spectrum for input, the good agreement obtained for this latter station (bottom left hand plot) simply verifies that the method is functioning correctly. Excellent agreement is also obtained for the outer nearfield positions (Y=8D) demonstrating that the objectives of the model are being met . At the inner near-field locations (Y=2D) some discrepancies are apparent between the measured and predicted spectra. However, the general agreement is still substantially good given that the predicted values are absolute and have not been adjusted empirically. At the downstream near-field station (X=4D), the discrepancy at low frequencies is probably due, at least in part, to the hydrodynamic field, which the results of Fig. 3 suggest would be relatively strong at this microphone location.

At stations close to the jet the assumption of grazing incidence, which is used to correct the microphone free field frequency response above 4kHz, could be an area for error since the sound waves are far from planar here. However, an area that is more likely to benefit from refinement concerns the possible axial variation of inherent directivity and longitudinal decay length scale (controlling convective amplification), which although treated as functions of Strouhal number are currently taken to be constant along the jet.

In the above test, the eddy convection speed is supersonic. However, at the Mach angle the model generates a radiation efficiency of unity and the Mach wave radiation is simply treated as jet mixing noise

within the model. In summary, Lighthill's classical theory, analysed in a frame of reference fixed relative to the nozzle, appears to provide a robust semi-empirical basis for predicting the near-field of jet mixing noise.

3.2 Shock Associated Noise

To compute the near-field of this jet noise component the phased linear array model of Ref. 11 is used. The model assumes that the shock noise is generated locally at the shock turbulence interaction sites formed at the end of each shock cell where a shock intersects the shear layer. The quasi-regular shock cell structure of an under-expanded supersonic jet is represented as shown in Fig 10, with the distance (L) between each source equal to the shock cell spacing, which reduces along the jet. The mirror measurements (Fig. 6) lend considerable credance to this discrete source structure. An important feature of the model is that adjacent sources are assumed to be correlated by convection of the turbulence, which retains some of its identity on passing from one shock to the next and sets the relative phase. This has two effects, firstly the characteristic frequency of shock noise, $f_p = U_c / \{L.[1 - M_c.\cos\theta]\}$ (Ref 11), reduces with increasing pressure ratio (Fig. 3) as a result of the shock cells lengthening and secondly, it exhibits a Doppler shift due to eddy convection. In Ref 11 a universal prediction scheme is derived, with the average shock spectrum and coherence (between adjacent cells) quantified through an analysis of far-field noise spectra. The overall intensity is shown to be a function of the Prandtl-Glauert factor β rather than jet velocity U_j, which controls jet mixing noise. This semi-empirical model of shock noise was adopted by the SAE as a standard prediction technique for aircraft engine noise (Ref. 12). Since the the work of Ref.11, studies have been undertaken to advance the physical understanding of shock noise (Ref. 13). However, for the acoustic analogy of the present work, the simple array model of Ref. 11 is considered adaquate.

With the shock noise source activity apparently concentrated at or close to those points where the shocks intersect the shear layer, for a round jet we may reasonably model the shock sources as annular regions of radius approximately equal to that of the nozzle as shown in Fig. 10a. Presuming that the azimuthal length scale of the source activity is similar to that of the turbulence then, as with jet mixing noise, for $r \geq D$ the equivalent point source array of Fig. 10b may be used to model the near-field of shock noise. Ignoring refraction etc caused by the flow, each source is assumed to be omnidirational and to have the relative strength indicated in Fig. 11a.

(a) 3D Source Structure   (b) Phased Point Source Model

Fig.10 Shock Noise Source Model

Measurements confirm that the length of the first cell is given by Pack's formula (Ref. 11): $L_1 = 1.31 D\beta$ where $\beta = \sqrt{M_j^2 - 1}$ is the Prandtl-Glauert factor (M_j being the fully expanded Mach number inside a cell - a function of pressure ratio only) and D is the nozzle exit diameter. In practice, losses across the shocks and the effect of jet mixing take their toll and the shock cells reduce in length in an approximately linear fashion along the jet to yield for the mth cell: $L_m = L_1 - [m-1].\Delta L$ where $\Delta L = \delta.L_1$ and $\delta \approx 0.06$ (the latter depends on the degree of screech present as this can have a significant effect on the jet mixing rate and also the number N of active shock sources). In the flight case, the shock cells lengthen.

For the static model of Fig. 10b, the acoustic pressure at any field point $\hat{z}$ is simply:

$$p(\hat{z}, t) = \sum_{m=1}^{m=N} \frac{F_m(x_m, t - \frac{r_m}{a_0})}{r_m}$$

(6)

where F_m, the equivalent acoustic monopole source fluctuation for the mth shock, is evaluated at the appropriate retarded time and N is the number of shock sources. In the absence of screech, N is typically eight for an underexpanded jet issuing from a convergent nozzle. To determine the power spectral density of the shock noise we Fourier transform the auto-correlation of eqn.6, which we express in the form:

$$A_p(\hat{z},\tau) = \sum_{m=1}^{N} \frac{1}{r_m} \sum_{n=1}^{N} \frac{\overline{F_m(x_m,t-\frac{r_m}{a_0})F_n(x_n,t+\tau-\frac{r_n}{a_0})}}{r_n} \qquad (7)$$

to subsequently obtain: $\quad G_p(\hat{z},\omega) = \sum_{m=1}^{N} \sum_{n=1}^{N} \frac{G_{mn}(\omega)}{r_m r_n} e^{j\omega\left[\frac{r_m-r_n}{a_0}-\tau_{mn}(\omega)\right]} \qquad (8)$

where $G_{mn}(\omega) = \left|\tilde{G}_{mn}(\omega)\right| = R_{mn}(\omega).\{G_{mm}(\omega).G_{nn}(\omega)\}^{\frac{1}{2}}$, G_{mm} being the psd of the mth source and R_{mn} the coherence of sources m and n, which by definition must lie in the range 0 to 1.0 (for m = n, R is of course equal to unity for all ω). The terms for which $m \neq n$ cause interference effects in the spectrum, with constructive interference producing the Doppler shifted peak f_p mentioned previously.

Eddy convection generates the phase delay $\tau_{mn}(\omega) = \frac{x_n - x_m}{U_c(\omega)}$ where for a static jet the eddy phase speed is $U_c(\omega) = \kappa_c(\omega).U_j$ while for the flight case, $U_c = U_a + \kappa_c(\omega).\{U_j - U_a\}$. The convection factor $\kappa_c(\omega)$ varies slowly with frequency about the group convection value (Fig. 11b), which is about 0.72.

Since there is little data on how R_{mn} varies with m and n, the average for the whole jet, derived in Ref. 11 (as a function of frequency), is currently used in the model. Denoting the average coherence between adjacent shocks by C_1 and assuming Gaussian decay, the correlation coefficient may be written: $R_{mn}(\omega) = \{C_1(\omega)\}^{i^2}$ where $i = |n - m|$.

When completed, the acoustic mirror study (Fig. 6) should provide detailed data on the strength of individual shocks as a function of frequency. In the mean time, the overall shock strength data of Fig. 11a, which was obtained by placing an acoustic shield next to the jet, is used. For this we define a normalised relative source strength S_m so that $G_{mm}(\omega) = S_m.\frac{G_0(1,\omega)}{N}$ and $\sum_{m=1}^{m=N} S_m = 1$

where $G_0(1,\omega)/N$ is the average shock source strength (for r=1 metre) and $G_0(1,\omega) = r_0^2 G_0(r_0,\omega)$.

The overall intensity of shock associated noise is given by $I = \frac{\overline{p}^2}{p_0^2} = K\left(\frac{D}{r_0}\right)^2 g(\beta) \qquad (9)$

For $\beta < 1.1$, $g(\beta) = \beta^4$ while for $\beta > 1.1$, the appearance of a Mach disc in the first cell results in a reduced dependence with $g(\beta) \approx \beta^{2.5}$.

The interference terms in eqn. 8 contribute little to the overall sound level and in order to satisfy eqn. 9, it can be shown that the source spectral density must be of the form:

$$G_0(r_0,\omega) = K_0.\left(\frac{D}{r_0}\right)^2.\frac{D}{a_0}.\beta.g(\beta).H_0(\sigma) \qquad (10)$$

The function H_0 can be regarded as the universal source spectrum of shock noise. Its apparent dependence solely on pressure ratio rather than say jet velocity is recognised here by assuming H_0 to be a unique function of a Helmholtz number $\sigma = fL/a_0$ rather than Strouhal number $St_{cell} = fL/U_c$. In fact, whilst the interference effects are velocity dependent through the peak frequency f_{p90} and the Doppler factor, there is no evidence that the characteristic frequency of individual shock waves is velocity dependent.

The universal generic parameters, H_0 and C_1, as originally evaluated in Ref. 11 for unheated round jets, are presented, slightly modified, in fig.11b. These average data were obtained through a least squares fit of eqn. 8 to the measured far-field variation with polar angle θ of the sound spectral density (corrected to remove mixing noise).
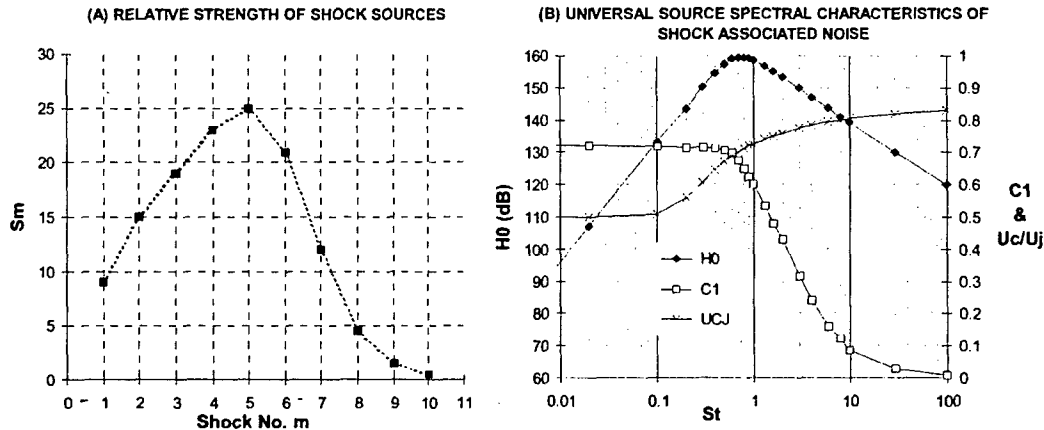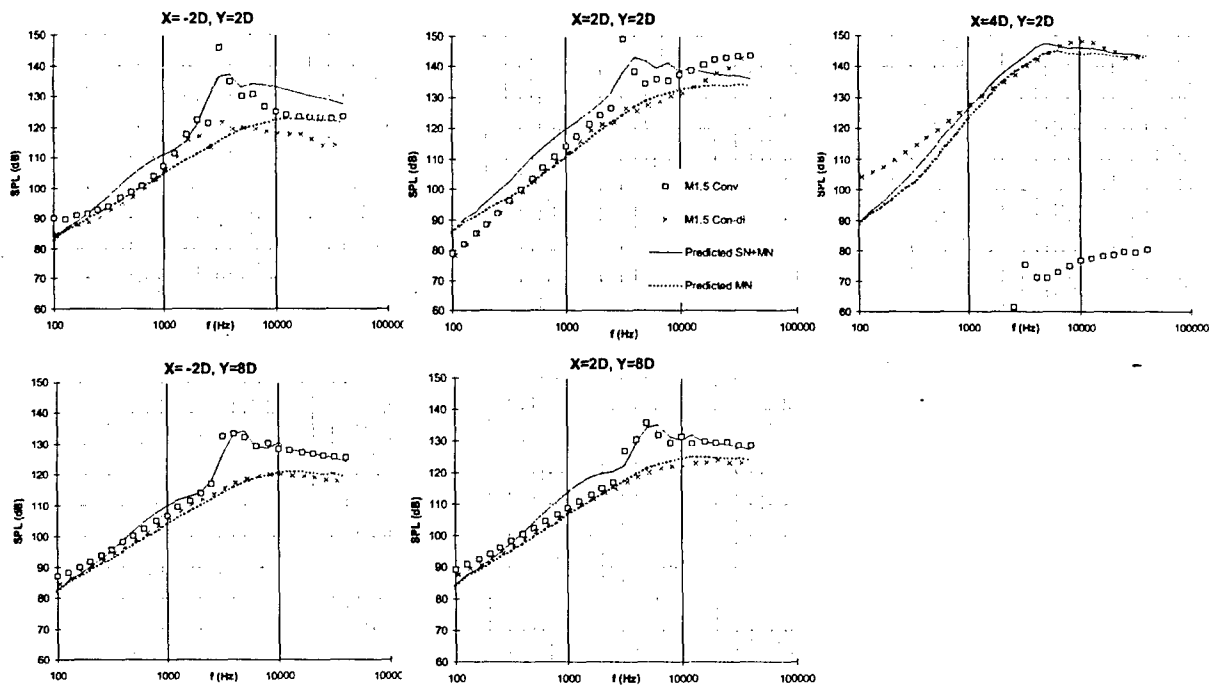
(A) RELATIVE STRENGTH OF SHOCK SOURCES

(B) UNIVERSAL SOURCE SPECTRAL CHARACTERISTICS OF SHOCK ASSOCIATED NOISE

Fig.11 Shock Noise Model Data

Fig.12 Shock Noise Predictions (M_j=1.5, T=885K, D=46mm Conical Nozzle)

The shock noise model is compared with measured near-field 1/3rd-octave spectra in Fig.12. For this test, which was also conducted in the NTF, the 39mm con-di nozzle was replaced with a convergent 46mm nozzle, and the five microphones were repositioned to retain the same X/D and Y/D values (Note that the downstream microphone malfunctioned in this test). Unfortunately, strong screech, which could affect the fidelity of the model, is visible in the data at the inner stations. Notwithstanding this, the degree of agreement between prediction and measurement is similar to that obtained for the mixing noise in Fig. 9. At the outer near-field stations reasonably good agreement is again obtained, while at the inner stations, discrepancies are once more in evidence. These should hopefully be rectified when more accurate information on the shock source strength as a function of frequency is available from the results of the acoustic mirror traverses referred to previously.

3.3 Spatial Coherence

The methodology used in deriving the jet noise near-field spectra has also been applied to predict the spatial coherence of the near-field noise. Knowledge of the spatial coherence is required in the correct assessment of airframe modal response.

The spatial coherence and phase for any two points $\hat{z}$ and $\hat{z}+\zeta$ in the noise field (Fig. 7) is obtained from the cross-power spectral density of the acoustic signals at the points, which we can determine from the Fourier transform of the cross-correlation of the signals, namely;

$$C_{12}(\tau) = \underset{T\to\infty}{Lt}\ \frac{1}{T}\int_0^T p_1(t).p_2(t+\tau)dt \quad \text{and} \quad \tilde{P}_{12}(\omega) = \frac{1}{2\pi}\int_{-\infty}^{\infty} C_{12}(\tau).e^{-j\omega\tau}d\tau \tag{11}$$

where τ is a time delay superimposed between the signals, C_{12} is the cross-correlation function and $\tilde{P}_{12}$ the (complex) cross-power spectral density (cpsd), which is conveniently expressed in terms of its modulus and phase:

$$\tilde{P}_{12}(\omega) = \left|\tilde{P}_{12}\right| \angle \tilde{P}_{12} = \sqrt{G_1(\omega).G_2(\omega)}.R_{12}(\omega).e^{j\omega\tau_p(\omega)}$$

R_{12} is the coherence of the two signals and τ_p the phase delay time. Typically, τ_p is a weak function of the frequency with a nominal value corresponding to the time delay at which the correlation function $C_{12}(\tau)$ peaks.

For jet mixing noise, inserting eqn.1 for the microphone signals in eqn. 11 and performing the Fourier transform we obtain, after some rearrangement, for the cross-power spectral density:

$$\tilde{P}_{12}(\omega) = G_{90}(\omega).\int_{y_1} D_{P_{12}}(y_1,\omega).C_{A_{12}}(y_1,\omega).S_0(y_1,\omega).e^{-jK[r_1-r_2]}\frac{dy_1}{r_1 r_2} \tag{12}$$

The principle difference between this result and the power spectral density of eqn. 3, is the presence of a diffraction exponential within the integral, involving the product of the wavenumber K of the sound and the path difference $r_1 - r_2$. A similar result is obtained for shock noise when the integral is then replaced by a double summation and the source strength is modified accordingly for S_m.
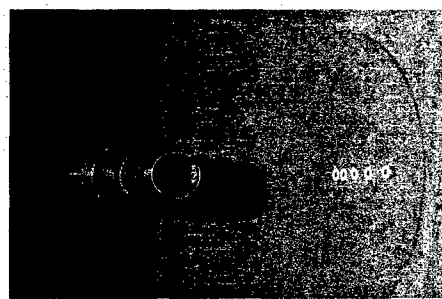
(a) Free Field Set-up   *(b) Semi-Free Field Set-up*

Figure 13. Model Scale Near-Field Jet Noise Tests on NTF Ground Rig

For a line source, such as jet mixing noise, which is spatially distributed relative to the wavelength of the sound, the diffraction exponential in eqn. 12 has a dispersive effect resulting in the decay of the coherence with increasing microphone separation. A single discrete source, shorter than say a quarter of a wavelength, would be acoustically compact and yield coherence $R_{12} \approx 1$ regardless of microphone separation. For multiple discrete sources separated spatially on a wavelength scale, such as shock noise, the coherence behaves in a complex manner comprising multiple peaks, not dissimilar to an optical diffraction pattern for a series of pin holes. In any event, the distributed nature of the sources has a significant effect on the coherence.

Finally, as with eqn.3, the factors D_p and C_A in eqn. 12 relate to the effect of inherent directivity and convective amplification but for two microphones in this instance. With the above exceptions, eqn. 12 is evaluated in exactly the same manner as eqn. 3, using the same generic source distribution data.
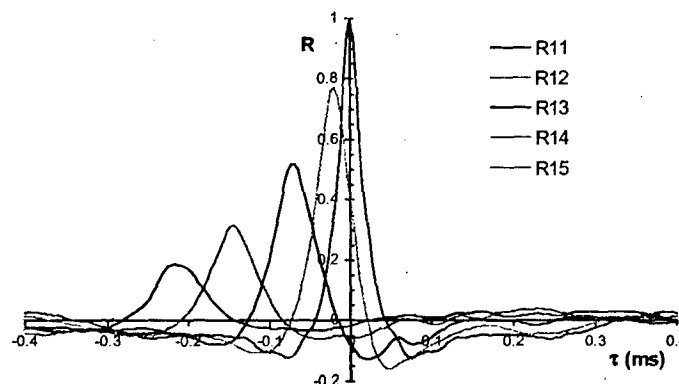

Figure 14. Near-Field Cross-Correlations for Model Scale Jet in the NTF

Model Scale Tests

To investigate near-field spatial coherence, a 2D long linear array of five (6.3mm B&K) microphones was employed (Fig. 13a), with relative spacing between microphones increased progressively along the array to compensate for the lower rate of decay of correlation of the low frequency components of jet mixing noise. Similar tests were also made for a semi-free field environment (Fig 13b) using a large rigid board adjacent to the jet with flush mounted microphones.

The microphone signals were acquired digitally using a sampling rate of 250Khz and appropriate anti-aliasing filters, for subsequent analysis off-line using software written in IDL (Interactive Data Language).
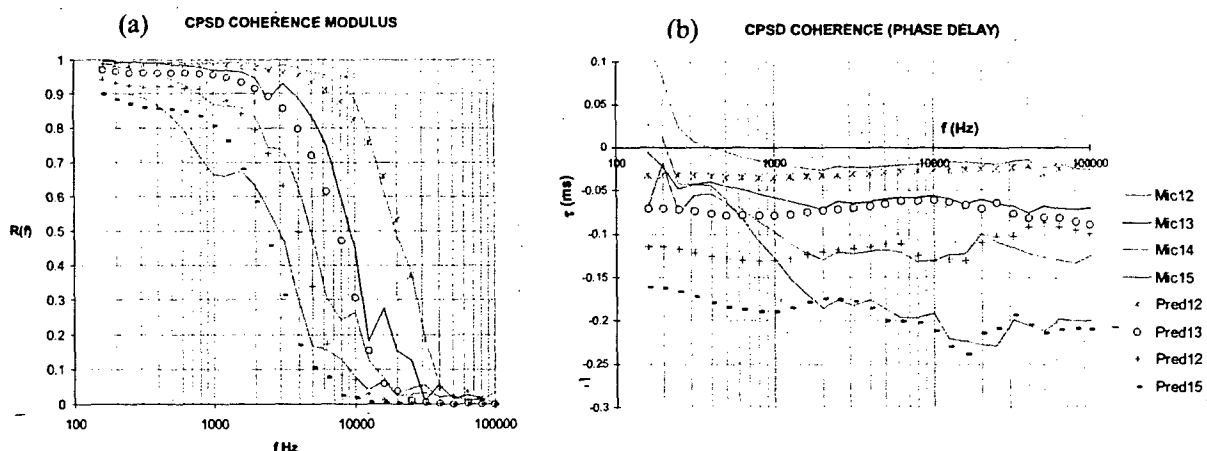
Figure 15 Model Scale Coherence and Phase Measurements Compared with Predictions

Typical cross-correlations at M0.9, for a free-field set-up are shown in Fig. 14. For this the array was parallel to the jet axis and offset 3.5D. Microphone 1 was aligned with the nozzle exit and the array arranged downstream. The signals of the downstream microphones have been delayed relative to microphone 1. It is seen that the correlations not only decay with increasing microphone separation but that peak correlation occurs at increasingly negative time delay, indicating that the sound is coming from a spatially extended noise source whose centroid is downstream of the array. These observations are in keeping with those expected of mixing noise radiated by the turbulent shear layer of the jet.

The coherence and phase for this test, determined in 1/3rd octave bands, is presented in Fig. 15 where they are compared with the predicted values obtained using eqn. 12. Referring to the coherence (Fig 15a), it will be seen that in general the predictions show good agreement with the measurements. As expected for a pure jet mixing noise source, the level of coherence reduces with increasing separation of the microphones and

also decreases with increasing frequency. At frequencies above about 50kHz (model scale) the correlation is virtually zero for all microphone separations. At this frequency the wavelength of the sound is around 7mm or 15% of nozzle diameter and the separation between microphones 1 and 2 was 15mm i.e. about two wavelengths at this frequency.

Turning to the phase information (Fig 15b), it will be seen that the agreement between measurement and theory is quite good above 2kHz where most of the energy resides, while below this frequency there is a growing discrepancy with reducing frequency, which is almost certainly due to the presence of the hydrodynamic near-field. In terms of phase angle, the error is quite small here being about 20 degrees at most, which is unlikely to be significant in airframe structural analysis.

Engine Tests

To provide data for initial validation of the near-field models applied to full scale engine applications, noise tests were conducted on a Spey turbojet engine in the QinetiQ GLEN sea-level engine test bed at Pyestock. Whilst far from ideal acoustically, the facility (used for engine controls development and validation) provided an important opportunity to obtain near-field noise measurements on a military turbojet engine for preliminary confirmation of the maths models at full scale.
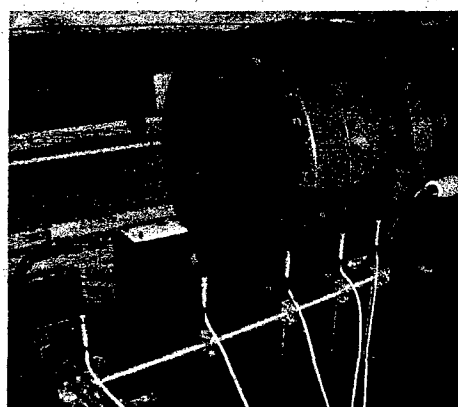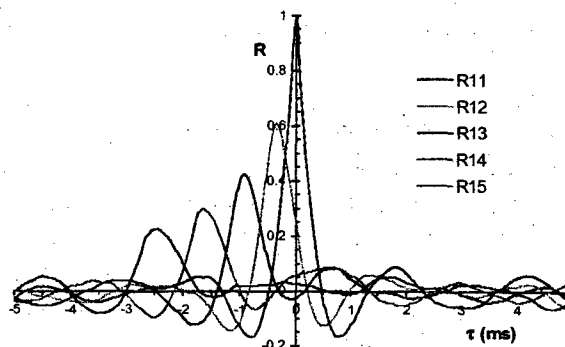

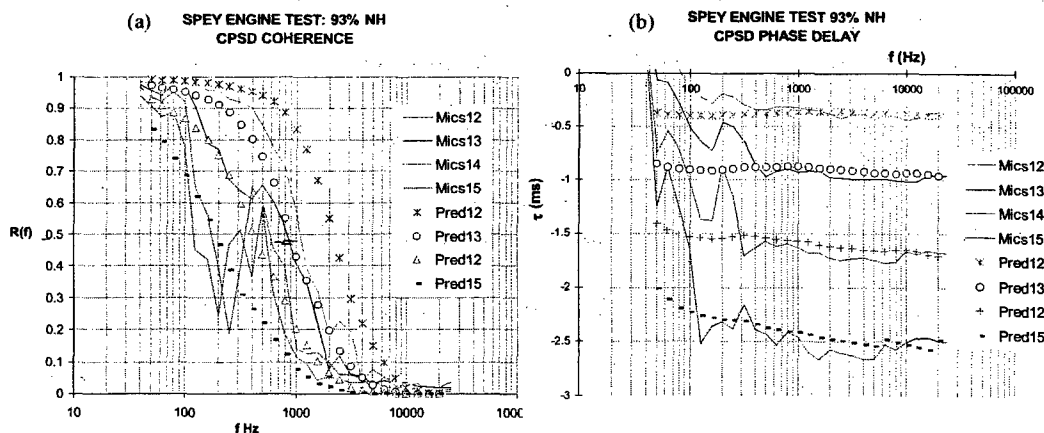Figure 16   Noise Tests on Spey Engine in QinetiQ GLEN Sea-Level Test Facility

Figure 17. Engine Coherence Data

A scaled up version of the linear microphone array used in the model scale tests was employed but offset from the engine axis by only 1.4D to minimise the effect of reflections. A set of typical cross-correlations for the five microphone array is shown in Fig.16 for the engine run at 93%N_H. The associated coherence and phase measurements are presented in Fig 17 along with predictions made using the maths model, eqn 12 above. An exhaust diffuser duct (not visible in the photograph of Fig.16) was located 3 diameters downstream of the nozzle exit plane. Significant flow entrainment by the jet exhaust in the diffuser would be expected to result in stretching of the source distributions, which could account for the measured coherence

decaying more rapidly with frequency than predicted in Fig. 17a. The close proximity of the diffuser to the engine would have resulted in shielding of the downstream jet noise sourceses from the microphone array, which combined with the hydrodynamic field would account for the discrepancies in the phase below 300Hz in Fig. 17b. In summary, the measured overall trends in the engine test appear to be predicted well by the maths model with the discrepancies between the two largely attributable to the test environment. Although not ideal, the tests have nevertheless served a useful basis for initial validation of the near-field maths models on a full scale application, permitting their further development and refinement.

Concluding Remarks

A semi-empirical basis for predicting the spectral intensity and spatial coherence of the jet noise field adjacent to the supersonic exhausts of turbojets has been described. The methodology adopted marries the acoustic analogy with source location measurements and encompasses both jet mixing noise and broadband shock noise. It has been tested on both model scale heated supersonic jets and through engine measurements. Excellent agreement is being obtained between prediction and measurement for outer near-field stations of the jet. At stations very close to the jet, the overall levels are replicated well by the models but further work is required to refine the fidelity for these stations, notably at the higher frequencies. Extension of the models to include the hydrodynamic field is planned, to improve prediction at low frequencies close to the jet.

Acknowledgements

References

1. P D GREEN, 'Current and Future Problems in Structural Acoustic Fatigue' AGARD-CP-549, Impact of Acoustic Loads on Aircraft Structures, May 1994.

2. R A PINKER, 'A Brief Review of the Source Noise Technology Applicable to Fixed-Wing Military Aircraft', AGARD-CP-512, Combat Aircraft Noise, October 1991.

3. COMET/Acoustics: Computational Mechanics Tool, Automated Analysis Corporation

4. M HARPER-BOURNE, 'Radial Distribution of Jet Noise Sources Using Far-Field Microphones', AIAA Paper 98-2357, Toulouse, June 1998.

5. M J FISHER, M HARPER-BOURNE AND S A L GLEGG, 'Jet Noise Source Location: the Polar Correlation Technique', Journal of Sound and Vibration, vol. 51, 1977.

6. M J LIGHTHILL, 'Jet Noise', AGARD Specialists' Meeting on "The Mechanism of Noise Generation in Turbulent Flow", Rep 448, 1963.

7. S E WRIGHT, 'An Advanced Course in Noise and Vibration', Institute of Sound and Vibration Research, University of Southampton, Chapter 1, Theory of Sources, Sept 1972

8. C L MORFEY, 'Amplification of Aerodynamic Noise by Convected Flow Inhomogeneities', Journal of Sound and Vibration., vol 31, 1973.

9. M HARPER-BOURNE, 'Jet Near-Field Noise Prediction', AIAA Paper 99-1838, Seattle, May 1999.

10. M HARPER-BOURNE, 'Twin Jet Near-Field Noise Prediction', AIAA Paper 2000-1838, Moui, September 1999.

11. M HARPER-BOURNE and M J FISHER, 'The Noise from Shock Waves in Supersonic Jets.', AGARD-CP-131, Noise Mechanisms, September 1973.

12. 'Gas Turbine Jet Exhaust Noise Prediction', SAE Aerospace Recommended Practice ARP876 Rev D. 1994.

13. TAM C.K.W., 'Supersoinc Jet Noise', Annual Review of Fluid Mechanics, vol 27, 1995.

List of symbols

a_0	Ambient speed of sound
ASTOVL	Advanced Short Take Off and Vertical Landing
B&K	Bruel and Kjaer
BEM	Boundary Element Method
BVR	Beyond visible range
C_A	Eddy convection factor

Con-Di	Convergent-divergent nozzle
D	Nozzle diameter (mm)
D_p	Source inherent directivity
f	Frequency (Hz)
FE	Finite element
G	Power spectral density
GLEN	Ground Level ENgine (test facility)
Hz	Cycles per second
IDL	Ineractive Data Language
K	Wavenumber ($= 2\pi / \lambda$)
L_1	Eddy axial decay length scale (mm)
λ	Wave length of sound
M_c	Eddy convection Mach number
M_j	Jet Mach number
N_H	High speed shaft relative speed
NTF	QinetiQ Pyestock anechoic Noise Test Facility
p	Acoustic pressure
P	Cross-spectral Density
PR	Pressure Ratio (Total pressure/ambient pressure)
RAM	Radar Absorbent Material
r	Sound propagation distance (m)
R	Coherence modulus
S	Source strength
s_d	Doppler shifted Strouhal number ($= \omega L_1 / U_c$)
SPL	Sound Pressure Level
t	Time (s)
T	Signal averaging time (s)
τ	Time delay (ms)
τ_p	Phase delay time (ms)
θ	Angle to jet axis
U_c	Eddy convection velocity (m/s)
ω	Radian frequency ($= 2\pi f$)
x	Far-field co-ordinate (m)
y	Source co-ordinate (m)
z	Near-field co-ordinate (m)